Journal of the European Ceramic Society 20 (2000) 913–926

Microstructure and phase transformations in the AlN–Al_2O_3 pseudo-binary system

P. Tabary[a], C. Servant[b,*], J.A. Alary[a]

[a]*Laboratoire de Métallurgie Structurale, URA CNRS 1107, Université de Paris-Sud, 91405 Orsay-Cedex, France*
[b]*Société Péchiney Electrométallurgie, Usine de Chedde, 74000 Le Fayet, France*

Received 28 June 1999; received in revised form 30 August 1999; accepted 12 September 1999

Abstract

The microstructure and phase transformations in the AlN–Al_2O_3 pseudo-binary system of samples having an AlN content in mol% ranging between 44 and about 0 are reported as a function of the thermal treatments. The nature of the phase equilibria, temperature and composition range and coherence degree of the different phases were studied by using various complementary experimental techniques.

Keywords: AlN–Al_2O_3; Al_2O_3; Microstucture-final; Phase equilbria

1. Introduction

The Alons, compounds of Al, N and O in the AlN–Al_2O_3 pseudo-binary section are used as abrasive materials. Several experimental and calculated assessments of the pseudo-binary section have been made but the nature of the phase equilibria, the stability and reversibilty of the different phases were subject to controversies. In addition, few papers present the microstructures of the phases. We studied recently the crystalline structures of the φ′ and δ phases by X-ray and neutron diffractions[1,2] and proposed a structural model which gives account for the double modulation in composition and displacement for both phases and which has been supported by high resolution electron microscopy experiments.[3] Taking into account this structural modelling, a sublattice thermodynamic modelling of those phases was made and a new version of the pseudo-binary section of the AlN–Al_2O_3 was calculated[4] and compared with previous ones which did not take into account the φ′ and/or δ phases. The present paper largely deals with the microstructures of the phases in the AlN–Al_2O_3 pseudo-binary section submitted to different thermal treatments, in order to understand their transformations.

2. Experimental

The elaboration of the Alons by the Péchiney Electrométallurgie Society consists of two steps. The first one is a reaction between aluminium (26 wt%) and alumina under flowing nitrogen at ~1 at, around 1273 K then at temperature higher than 1623 K, which gives a product labelled "Alon roche" with 50 AlN and 50 Al_2O_3 (in mol%). During the second step, the "Alon roche" is ground, then mixed with alumina with variable content in order to obtain samples with AlN content ranging from 50 to about 0 (in mol%), and finally melted under air in an arc furnace. The cooling may be slow ($R_c = 15$ K min^{-1}, estimated between 2373 and 1773 K) inside the furnace or fast ($R_c = 500$–1000 min^{-1}) when the liquid solidifies on a cold metallic sheet. The composition of the samples determined by chemical analyses is listed in Table 1.

The samples were studied by several characterization techniques: X-ray, neutron, electron diffractions and optical (OM), scanning electron (SEM), transmission electron (TEM) microscopies. By SEM, the two types of contrast (chemical and topological) are the best by using back-scattered electrons. In the case of the chemical contrast, the grey level is inversely proportional to $\bar{Z}_{vol}$ (average volume number) equal to:

$$\bar{Z}_{vol} = \frac{\rho}{\bar{M}_{at}} \bar{Z}_{at}$$

* Corresponding author.
E-mail address: colette.servant@metal.u-psud.fr (C. Servant).

0955-2219/00/$ - see front matter
PII: S0955-2219(99)00238-1

Table 1
Composition of the samples considered in the present work

Sample no.	Chemical composition (weight %)						Composition (mol% AlN)	
	Al	O	N	C	Fe	Si		Mean value
1	56.1	38	8–8.95	0.26–0.43	0.3	0.27	41.9–44.7	43.3 ± 2.2
2			6.38					36.3 ± 1.8
3	55	40	4.6–5.23	0.14	0.4	0.25	28.3–30.9	29.6 ± 1.5
4	55.2	41	4.5 — 4.88	0.72	0.38	0.24		28.2 ± 1.4
5	54.4	43	3.4	0.57	0.21	0.23		21.3 ± 1.1
6	53.7–54.3	46–44	1.6–1.5	0.35–0.15	0.14	0.1	10.65–10.46	10.55 ± 0.5
7	53.4	45	0.5	0.94				3.5 ± 0.2

with $\bar{Z}_{at}$, and $\bar{M}_{at}$, respectively, the average atomic number and mass of the phase and ρ its volume mass.

Theoretically, two phases having $\Delta\bar{Z}_{vol} = 1\%$ can be separated. We calculated $\bar{Z}_{at}$ $(Al_2O_3) = \bar{Z}_{at}$ $(AlN) = 10$ and $\bar{M}_{at}(Al_2O_3) \sim \bar{M}_{at}(AlN) \sim 20.45$, therefore $\bar{Z}_{at}$ and $\bar{M}_{at}$ are practically constant along the pseudo-binary section Al_2O_3–AlN and $\bar{Z}_{vol}$ is directly related to the volume mass of the phases. In Table 2, are listed the contrasts of the different phases as well as their theoretical volume mass and the topological position of the phases compared to the γ-Alon spinel matrix.

Practically, the 27R, 21R and 12H polytypes appear with the same contrast by SEM but brighter than AlN. The φ′ and δ phases, having the same contrast, cannot be distinguished but can be separated from γ. The corundum must appear brighter than all the other phases due to its chemical contrast: this is observed on small areas; but as its hardness is higher than the one of all the other phases, on large areas (some μm^2) it appears raised and with a darker topological contrast. By using the optical microscopy, the contrast is inverse to the SEM one and the γ, φ′ and δ phases cannot be separated.

The phase transformations were followed by scanning differential thermal analysis in a device type SETARAM-TAG 24. The heating rate ranged between 30 and 10 K min^{-1} and was exclusively 30 K min^{-1} for annealings at temperature higher than 2423 K in order to limit the composition changes and the weight losses. The cooling rate might range between 1 and 99 K min^{-1}, but in general after the melting peak, the cooling rate used was 10 K min^{-1} down to 2273 K, the temperature at which the furnace was stopped. The atmosphere used was argon at ~1 atm because we have shown that nitrogen reacts with the 95%W–5%Re/74%W–26%Re thermocouples in particular for temperatures higher than 2173 K and therefore would have given erroneous temperature data. Pure corundum was used as a standard for the melting temperatures (2327 K) and the enthalpy of melting ($\Delta H = 1054$ kJ/g).

The weight fraction of the components of the eutectoid reactions involving the 12H and 21R polytypes were determined by X-ray diffraction performed at room temperature. First by assuming the ions Al^{3+}, O^{-2} and N^{-3}, so with the identical electrical charge equal to 10 e-, and secondly by neglecting small variations due to the low differences in the interreticular distances, the intensities of the X-ray diffraction peaks $(00\ 12)_{12H}$, $(00\ 21)_{21R}$ and $(002)_{AlN}$ must satisfy the following relations of the structural model of Jack[5]:

$I_{(00\ 12)}(12H)/I_{(002)}(AlN) = (6^2 + 5^2)/(6^2 + 6^2) = 0.85$ for n_{Al} = constant, (or 0.79 for weight = constant)

$I_{(00\ 21)}(21R)/I_{(002)}(AlN) = (7^2 + 6^2)/(7^2 + 7^2) = 0.87$ for n_{Al} = constant, (or 0.81 for weight = constant)

$I_{(00\ 12)}(12H)/I_{(00\ 21)}(21R) = 0.98$ for n_{Al} = constant

Table 2
Contrast of the phases in optical and scanning electron microscopies and their topological position versus the γ-Alon spinel matrix

Phases	Grey level (+dark↔bright)		$\rho_{theoretical}$ (g/cm^3)	Position versus γ-Alon spinel matrix
	O.M.	S.E.M. (back-scattered electron)		
AlN	+	+ + + +	3.26	Recessed
27R	+ +	+ + +	3.26	Recessed
21R	+ +	+ + +	3.325	Recessed
12H	+ +	+ + +	3.306	Recessed
γ	+ + +	+ +	3.68	
φ′	+ + +	+	3.68	Same level
δ	+ + +	+	3.67	Same level
α-Al_2O_3	+ + + +	Variable	3.97	Raised

The weight fractions of the different phases involved in the reactions (4)–(6), defined in Section 3.2.1, can be calculated from the intensities of the X-ray diffraction peaks as follows:

$$y(4) = \frac{I_{(0021)}(21R)}{I_{(0012)}(12H) + 0.944.I_{(0021)}(21R)} \quad (1)$$

$$y(5) = \frac{(0.79/0.559).I_{(002)}(AlN)}{(0.79/0.559).I_{(002)}(AlN)+I_{(0012)}(12H)} = \frac{I_{(002)}(AlN)}{I_{(002)}(AlN) + 0.71.I_{(0012)}(12H)} \quad (2)$$

$$y(6) = \frac{I_{(002)}(AlN)}{I_{(002)}(AlN) + 0.745.I_{(0021)}(2IR)}, \quad (3)$$

with $y(n)$ = transformed weight fraction at time t for the reaction noted (n).

Taking into account the important number of reactions studied, we assumed that the FWHM (Full Width at Half Maximum of intensity) of the X-ray diffraction peaks $(00\ 12)_{12H}$, $(00\ 21)_{21R}$ and $(002)_{AlN}$ was identical. So, the intensity of the X-ray diffraction peaks was identified with their height. In order to take into account the effects of texture, three X-ray diffraction spectra were recorded on each specimen and the transformed weight fraction $y(n)$ for a (n) reaction was therefore an average value.

3. Results and discussion

First, by X-ray diffraction, optical and scanning electron microscopies, we have characterized roughly the volume fraction of the different phases present in the samples. Then a quantitative measurement of the weight fraction of the phases was carried out in some samples by the Rietveld profile refinement analysis[6] of the neutron diffraction peaks, (see Table 3), with the use of a more important wavelength (2.426 Å) than with X-ray (in order to separate overlapping peaks) on the G41 spectrometer of the Laboratoire Léon Brillouin of the Centre d'Etudes de Saclay and the program Fullprof.[7]

We have observed that the cooling rate has no influence on the presence of the phases γ,φ′,δ and α-Al_2O_3. On the contrary, in the case of the sample 1, the presence of the phases AlN, 21R and 27R depends strongly on R_c (see Table 4).

In order to maintain metastable the 27R polytype at room temperature, R_c must be higher than 700 K min^{-1}.

3.1. Morphology and coherence of the phases

3.1.1. Polytypes

On a plane section of sample 1 water quenched, the 27R polytypes appear as needles distributed at random [Figs. 1(a) and (b)]. From electron micrographs, Jack[5] proposed a lath morphology for the 15R polytype in a β-SiC (hexagonal) matrix, and Sakaï[8] a plate morphology for the 27R polytype in an hot-pressed AlN matrix. The examination of sample 1 did not allow a choice between these two possibilities; it can only be noted that the c axis of the hexagonal cell of the polytypes is always perpendicular to the length of their needles, so these latter are more probably discs (or hexagons) with a diameter much more important than their thickness.

When the number of discs per unit volume is low, their diameter is close to the size of the grains of the γ-Alon spinel phase (up to 1 mm for a 40 μm thickness). When it is increasing, their mean diameter decreases

Table 4
Influence of the cooling rate on the polytype type

R_c (K min^{-1})	> 700	700–100	100–5	< 5
Present phase	27R	27R + 21R	21R + AlN	AlN

Table 3
Phases characterized in the samples studied[a]

Sample number	Cooling rate (R_c)[b]	AlN-21R-27R	γ	φ′	δ	α-Al_2O_3
1	Slow	+ (7.8) AlN + 4.2 (21R)	+ + + + + + + + + (88.0)	Traces		
4	Slow	Traces	+ + + + + + + + +	+		
5	Slow		+ + + + + + (56.7)	+ + + + (42.1)		(1.1)
6	Slow		+ (3.5)	+ + + + + + + + + (85.9)	+ (4.4)	+ (5.9)
7	Fast				+ + + + + + + + + (84.5)	+ + (15.4)

[a] The number of +, determined by X-ray diffraction, OM and SEM, was roughly proportional to the volume fraction of the phases, and the weight fraction (in %) indicated between brackets was measured with more precision by neutron diffraction.

[b] R_c noted slow and fast was respectively equal to 15 and 500–1000 K min^{-1}.

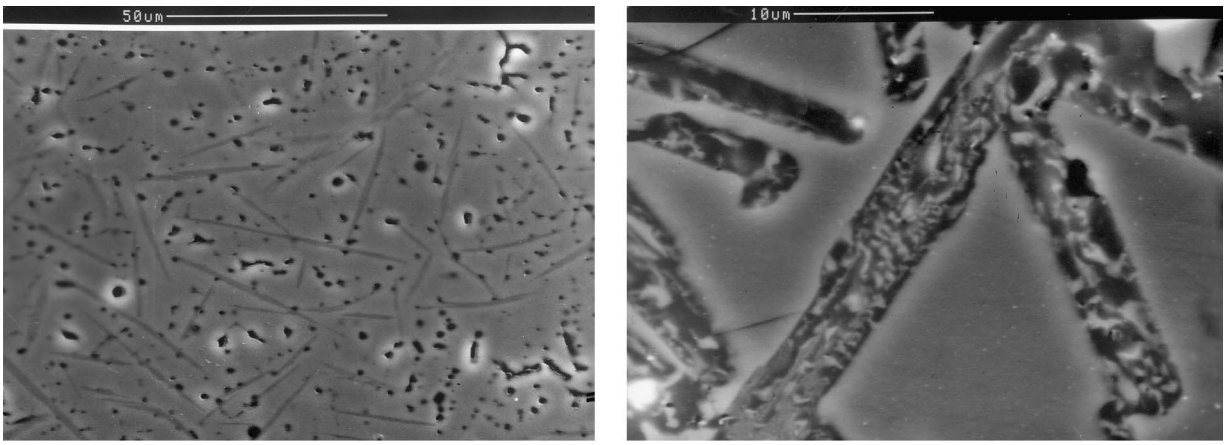

Fig. 1. (a) Optical micrograph at low magnification of sample 1, water quenched, showing the 27R polytype inside a γ-Alon matrix; (b) scanning back-scattered electron micrograph of sample 1, water-quenched, showing 27R polytype needles eutectoidally decomposed into AlN + γ-Alon.

because their side growth is stopped by the development of other discs, but the ratio diameter/thickness is somewhat constant. The polytypes are present either in the γ-Alon grain boundaries or inside the γ-Alon grains.

The following orientation relationships were determined between the 27R, 21R polytypes and the γ-Alon spinel matrix (Figs. 2 and 3):

$$(001)\gamma//(001)_{27R} \text{ with } \theta([220]^{*}\gamma, [100]^{*}_{27R}) = \theta([110]\gamma, [210]_{27R}) \sim 9^{\circ} \quad (4)$$

$$(5\bar{5}3)\gamma//(001)_{21R} \text{ with } \theta([220]^{*}\gamma, [100]^{*}_{21R}) = \theta([110]\gamma, [210]_{21R}) \sim 7^{\circ} \quad (5)$$

In any case, the habit plane between the polytype/γ-Alon spinel phases is the (001) dense plane for the polytype whereas the {111} dense planes for the γ-Alon spinel are not habit planes. Nevertheless, a [110] dense direction of the γ-Alon spinel belongs to the interface, but is not parallel to the [100] dense direction of the polytype.

At low temperature, the polytypes are partly or entirely decomposed in AlN + γ-Alon spinel by a eutectoid reaction.

3.1.2. Eutectoid AlN + γ-Alon

Two morphologies of eutectoid, noted A and B, have been observed in sample 1 slowly cooled at $R_c = 15$ K min^{-1}, Figs. 4(a) and (b) and Figs. 5(a) and (b). Their growth starts at the interface γ-Alon spinel/polytypes and extents in the whole volume of the polytype. It has been noted that AlN is present in sample 1 only in the decomposed disks of the 21R polytype Fig. 2(a). In this sample, the average decomposition ratio of the polytype by the eutectoid reaction 21R→AlN + γ-Alon spinel was 75.5 in wt%, so the weight fraction of 21R in sample 1 before the eutectoid decomposition was therefore 17%.

3.1.2.1. Eutectoid A. The eutectoid A often presents a disorganized feature with short lamellae parallel to the edges of the polytype plate. The average interlamellar distance of the eutectoid A is about 200 nm. In some parts, it appears coarser, maybe due to the coarsening of the phases.

In Fig. 6(a) and (b) are respectively shown the electron micrograph and the diffraction pattern which leads to the determination of the following orientation relationship:

$$(111)\gamma//(001)_{21R}//(001)_{AlN} \text{ with } [2\bar{2}0]\gamma//[010]_{21R}//[010]_{AlN} \quad (6)$$

In this case, the habit planes are the dense planes of each phase, even for the γ-Alon spinel phase, in opposition to relations (5) and (6) where the γ-Alon spinel was the matrix and not a product of the eutectoid reaction inside a polytype. In the case of γ-Alon spinel present in the A eutectoid, two variants symmetrical versus [111]γ are observed which are deduced the one from the other by a 60° rotation around the [111]γ direction. They correspond to two different packings of the f.c.c. phase: either ABCABCAB... or ACBACBAC..., the interface plane A being not modified. The fact that the eutectoid A forms from the 21R parent phase with an orientation relationship is unusual.[9]

The misfit between the different phases is reported in Table 5. It has been calculated with a γ-Alon spinel crystalline parameter equal to 7.945 Å. Note the better coherence between 21R/AlN than between 21R/γ-Alon spinel. In fact, in some eutectoid plates, two domains may be distinguished in the thickness of the plate; the upper part occupying a more important volume may be related to AlN Fig. 6. This hypothesis is confirmed by the observation of "moiré" fringes, parallel to the side of this upper part, which is in agreement

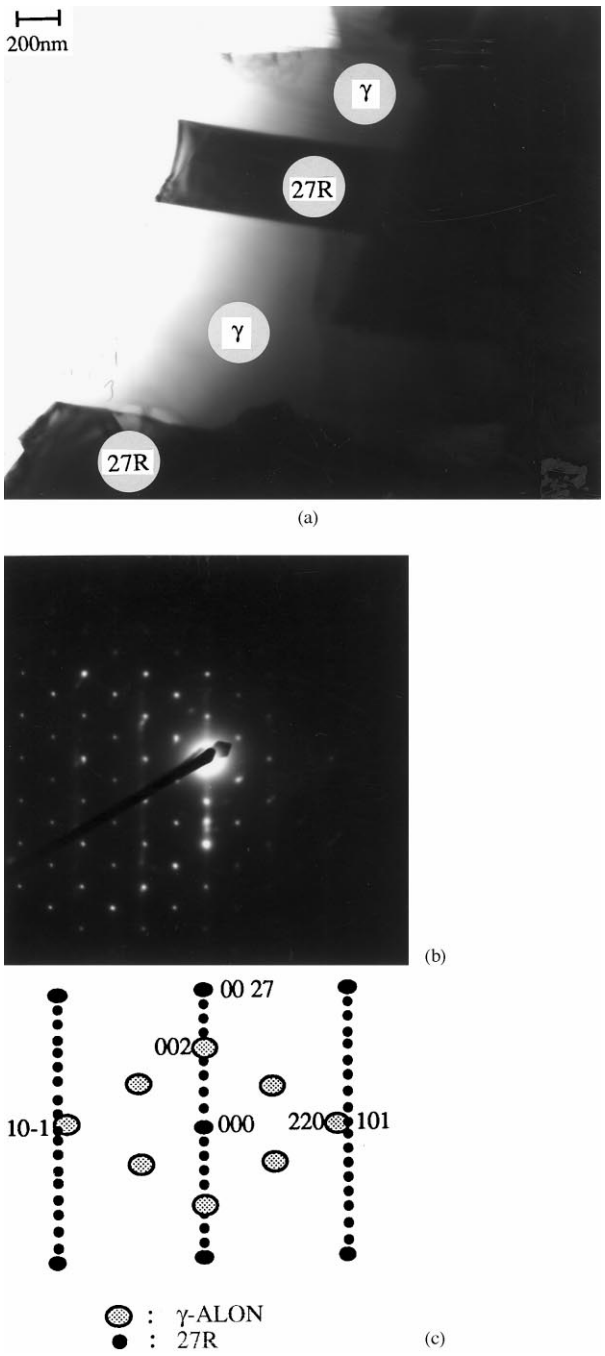

Fig. 2. Sample 1 water quenched ($R_c > 700$ K min^{-1}) (a) bright field electron micrograph showing the orientation of the disks of 27R polytype versus the γ-Alon matrix, (b) electron diffraction pattern showing the orientation relationship between the 27R polytype and the γ-Alon matrix, (c) schematic representation of (b).

with the less important calculated misfit between 21R and AlN ($\delta = -2\%$). As the interface between AlN and γ-Alon spinel is not perfectly plane, this may be due to the lesser coherence (10.2%) between their lattices, a badly defined eutectoid morphology is observed when the polytype matrix is entirely decomposed. Furthermore, the value of the average misfit in the interface plane (5%) and perpendicularly (12%) can explain the plate morphology of the eutectoid.

3.1.2.2. Eutectoid B. In the eutectoid B, the lamellae are generally well organized with several systems of branching. Contrary to the eutectoid A, the orientation of the B eutectoid lamellar components versus the polytype parent phase plate is indifferent. The decomposition front seems to move perpendicularly to the polytype parent phase plate as usual in eutectoids and the interlamellar distance is 150 ± 50 nm. In Figs. 7(a) and b are shown the electron diffraction pattern and the corresponding micrograph from which the parallel interface planes can be deduced: (111)γ and (101)AlN. Only one variant was oberved for γ-Alon spinel, certainly because the electron diffraction pattern was recorded on eutectoid lamellae belonging to the same system of branching. In addition, we have verified that the orientation of the γ-Alon spinel matrix in sample 1 and the one of the γ-Alon spinel lamellae resulting of the eutectoid reaction in the parent phase polytype are different.

The major difference between the two types of eutectoid A and B is the existence or not of orientation relationship between the parent phase polytype and the components of the eutectoid reaction.

3.1.3. γ,φ′ and δ phases

3.1.3.1. γ/φ′. These phases are present in samples 1–7, (see Table 3). Their grains are equiaxed with a size varying with the cooling rate: 100 μm for a water quench ($R_c > 10\,000$ K min^{-1}), 250 mm for a fast cooling ($R_c > 700$ K min^{-1}) and 350 μm for a slow cooling ($R_c < 100$ K min^{-1}).

The γ/φ′ grain boundaries are often curved and do not exhibit relief contrast. The misfit between the two phases, calculated for the three directions of the cube $\delta_{(a,b,c)}\% \sim (0.8\ 0\ 1.2)$ by using the parameters $a_\gamma \sim =$ 7.935 Å and (a,b,c,α,β,γ) φ = (7.998 Å, 7.938 Å, 7.835 Å, 90°, 90.88°, 90°) shows that these two phases are coherent. Bassoul et al.[10] reported that non-stoichiometric spinels when decomposed at high temperatures, form an intermediate metastable phase noted ε (old notation for φ′). From our experiments, it seems more probable that φ′ forms from the residual liquid after the formation of γ. The scanning back-scattered electron micrograph of Fig. 8 shows the equiaxed φ′ phase grains in sample 6 slowly cooled ($R_c = 15$ K min^{-1}).

No eutectic morpholy γ + φ′ was observed and the equilibrium γ + φ′ + liquid might be as well as a peritectic one. In the calculated assessment of the AlN–Al_2O_3 pseudo-binary section, an eutectic reaction was kept.[4]

3.1.3.2. φ′/δ. Taking into account the small difference in parameters for the two phases: $(a,b,c,\alpha,\beta,\gamma)_{\varphi'}$ = (7.998Å, 7.938Å, 7.835Å, 90°, 90.88°, 90°) and

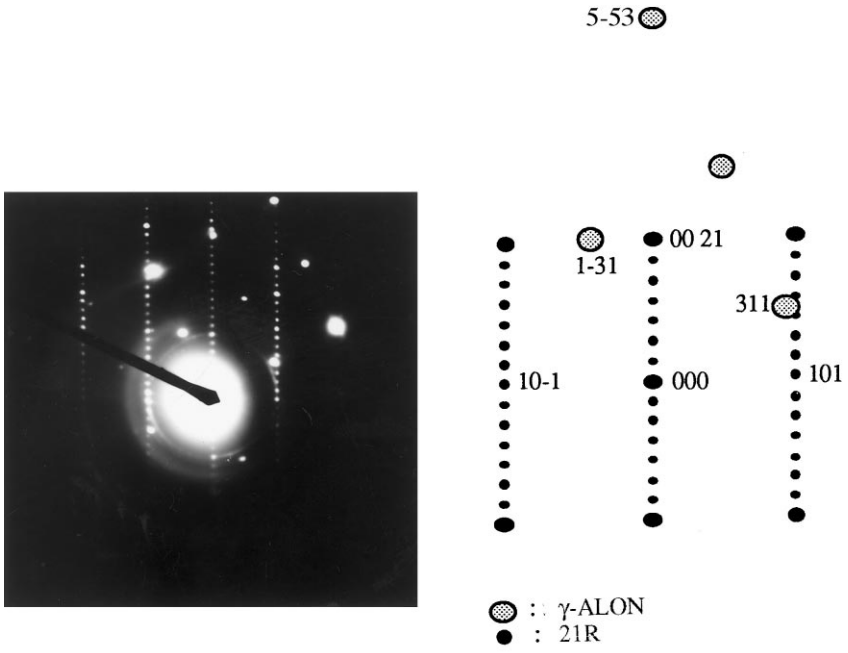

Fig. 3. Sample 1 slowly cooled ($R_c < 100$ K min^{-1}) (a) electron diffraction pattern showing the orientation relationship between the 21R polytype and the matrix; (b) schematic representation of (a).

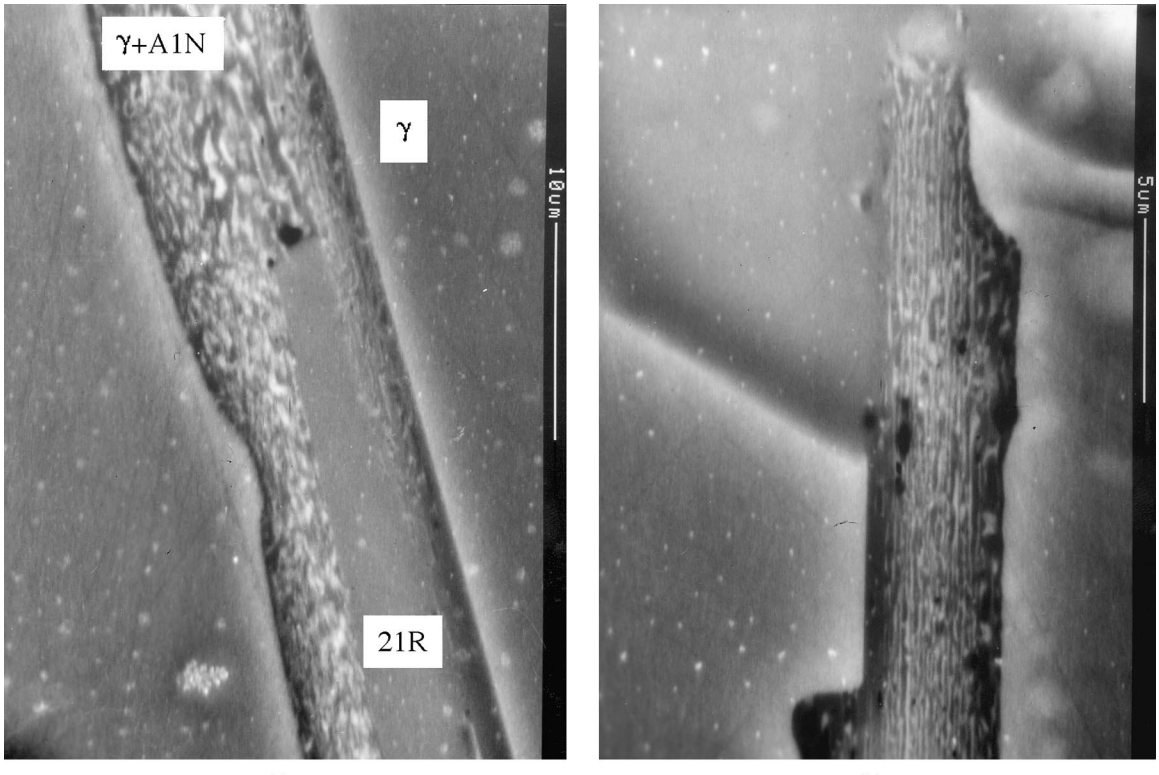

Fig. 4. Scanning back-scattered electron micrograph of sample 1, slowly cooled at $R_c < 100$ K min^{-1} showing: (a) 21R polytype lamellae eutectoidally decomposed partly into AlN + γ-Alon and (b) the A eutectoid lamellae growth parallel to the 21R polytype lamellae edges.

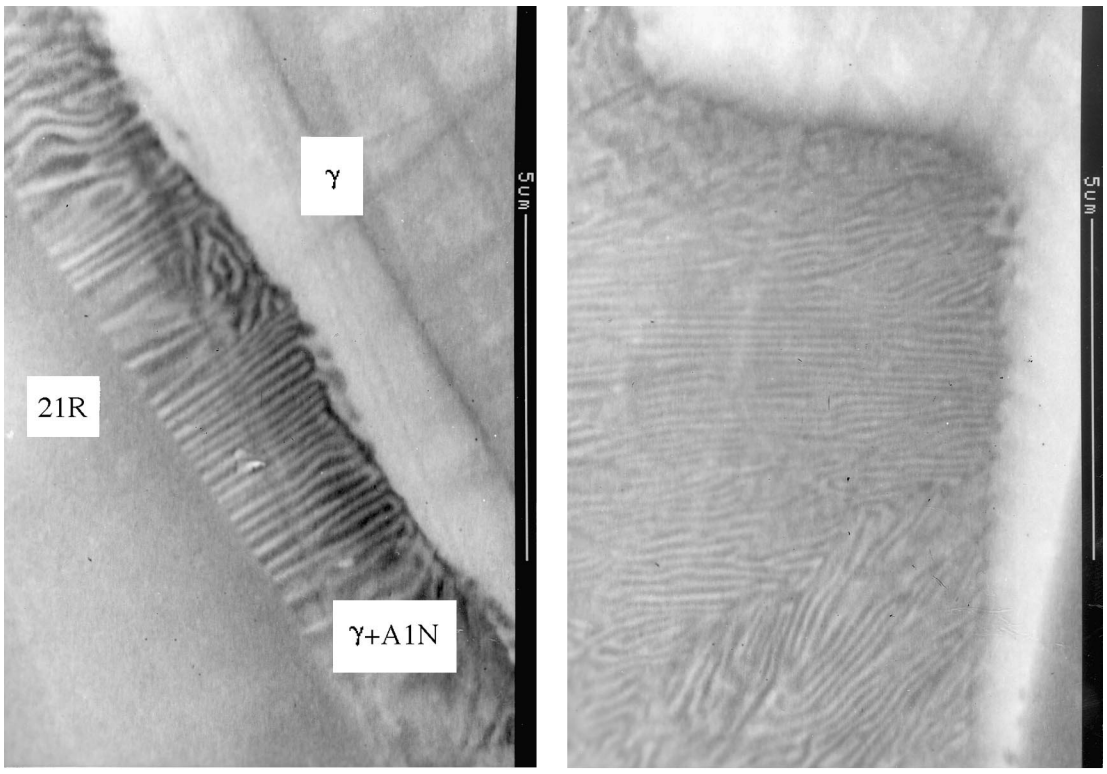

(a) (b)

Fig. 5. Scanning back-scattered electron micrograph of sample 1, cooled at $R_c < 100$ K min^{-1} showing: (a) 21R polytype lamellae eutectoidally decomposed entirely into AlN + γ-Alon; (b) it will be noted the branching of colonies in the B eutectoid.

$(a,b,c,\alpha,\beta,\gamma)_\delta = (7.963$ Å, 7.932 Å, 7.814 Å, 90°, 90°, 90°), the greatest misfit was calculated equal to 2.3%, and it seems highly probable that the δ phase precipitates coherently or semi-coherently from φ′.

3.1.4. δ/α-Al_2O_3

The scanning back-scattered electron micrographs of Figs. 9 and 10 show the δ and α-Al_2O_3 phases in sample 7 water quenched. The contrast of α-Al_2O_3 is darker than the one of δ. When the mole fraction of α-Al_2O_3 is low, that phase is localized at the grain-boundaries of the δ phase, the grain size of which ranges between 0.1 and 1 mm, (Fig. 9). When the mol fraction is more important, the α-Al_2O_3 phase appears as grains with 200 μm size, (Fig. 10). It can also precipitate as plates inside the δ grains. By considering the small cell of corundum: $a' = a\sqrt{3} = 2.747$ Å, and the $<110>$ directions belonging to the $(111)_\delta$ plane having (2.81 Å, 2.79 Å, 2.78 Å) as norms, the greatest misfit is equal to 2.2%). The $(111)_\delta$ plane is practically hexagonal with 1° deviation, so it is then normal to observe hexagonal or needle α-Al_2O_3 precipitates as a function of the δ section plane. The δ phase decomposes into φ′ + α-Al_2O_3 below 2258 K, as shown in Fig. 11 relative to sample 7 annealed at 2223 K during 1 h. In sample 6, enriched in nitrogen, the volume fraction of φ′ phase is higher than the one of α-Al_2O_3 the precipitation of which is intergranular, see Fig. 12 relative to sample 6 annealed at 2123 K during 1 h.

3.2. Stability and composition of the phases

On different specimens of sample 1 slowly cooled at $R_c = 15$ K min^{-1} (the start state of which is metastable two phased: γ-Alon spinel + 21R polytype; the stable state of the phase equilibrium diagram, consisting of AlN + α-Al_2O_3, never being reached), three types of thermal treatments were performed in the DTA device:

(i) A heating carried out at either $R_h = 10$ or 30 K min^{-1} (depending on the maximum temperature reached during this heating) immediately followed by a cooling at 100 K min$^{-1} > R_c > 5$ K min^{-1}. During the heating, the melting of the phases in the specimen is detected on the heat flow of the DTA curve by a peak more or less well defined.

In Table 6 is reported the temperature of the peak onset recorded on the heat flow curves of the different samples labelled 1 to 7. In the case of samples 1 and 2, it has been noted first a small change in the slope of the heat flow curve preceding the onset of the principal peak, which has been associated with a partial melting from microstructural observations and other annealings, secondly the peak corresponding to the γ-AlON spinel melting; the disks of polytypes (17 wt% remain solid). In the case of samples 4 and 5, the peaks are spread and for sample 5, two

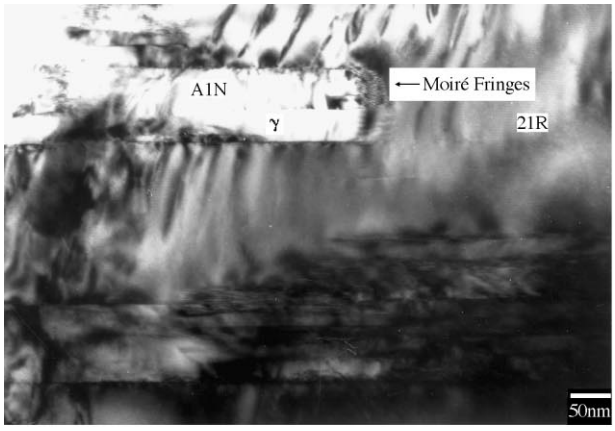

(a)

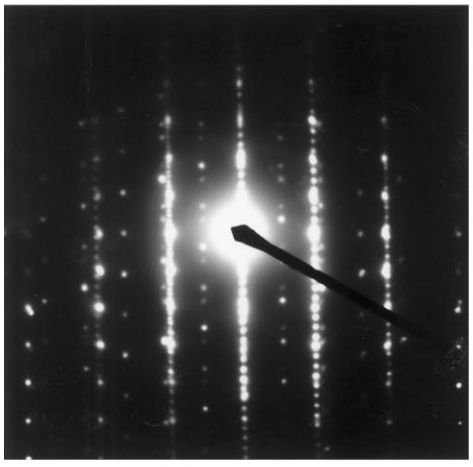

(b)

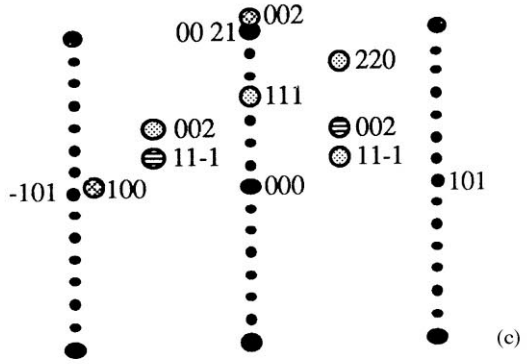

(c)

⊗ : γ-ALON (1rst variant)
⊜ : γ-ALON (2nd variant), symmetry axis [111]
● : 21R
⊗ : AlN

Fig. 6. Sample 1 slowly cooled ($R_c < 100$ K min^{-1}) (a) bright field electron micrograph showing the eutectoid A: AlN + γ-Alon in the 21R matrix; it will be noted the "moiré fringes" in the upper part of the eutectoid lamella. (b) electron diffraction pattern showing the orientation relationship between the 21R polytype, AlN and γ-Alon (two variants). (c) schematic representation of (b).

overlapping peaks are observed which respectively correspond to the φ′ then γ-Alon spinel melting. In the case of samples 6 and 7, the overlapping peaks are better defined and correspond to the successive melting of φ′ and δ-Alon.

(ii) Or a heating up to T_1, then an annealing at T_1 during which the kinetics of some phase equilibria were determined, followed by a cooling at $R_c > 100$ K min^{-1}.

(iii) Or a heating up to T_1, then a first annealing at T_1, followed by a cooling until T_2 at $R_c > 100$ K min^{-1}, then a second annealing at T_2, during which the phases formed at T_1 decompose, and finally a cooling to room temperature.

Table 5
Misfit between the parent phase 21R polytype and the components of the eutectoid A

δ (%)	21R/AlN	AlN/γ-Alon	γ-Alon/21R
$(111)\gamma//(001)_{21R,AlN}$	−2.0	+10.2	−8.2
$(2\bar{2}0)\gamma//(100)_{21R,AlN}$	+9.0	+8.0[a]	−17.1

[a] This type of interface was not observed.

The phases formed during these thermal treatments have been identified and their weight fraction has been determined by X-ray diffraction performed at room temperature.

3.2.1. Polytypes

The stability range of the polytypes was determined in the case of sample 1 (Metastable Start State, noted as MSS, composed of 21R + γ-Alon spinel).

During the annealings seven phase equilibria were observed (labelled between brackets):

1. 21R <–> 27R + liquid
2. 12H <–> 21R + liquid
3. 12H + γ-Alon <–> Liquid
4. 21R + γ-Alon <–> 12H
5. AlN + γ-Alon <–> 12H
6. AlN + γ-Alon <–> 21R
7. AlN + γ-Alon <–> 27R

3.2.1.1. Formation of the 27R, 21R and 12H polytypes from AlN + γ-Alon [reactions [(7), (6) and (5)], and decomposition. The stability domain of the different phases and the total duration to reach the phase equilibrium are indicated in the graph plotted in Fig. 13. In the stability range of AlN + γ-Alon is indicated the nature of the eutectoid formed by reaction (6) as (6A) or (6B). In a first step, it has been shown that after a heating up to 2163 ± 10 K followed by a 3 h annealing, AlN is stable, noted AlN S in Fig. 13. It begins to decompose above 2183 ± 10 K. After a 1 h annealing at this temperature, the polytype weight fraction is too small to identify the nature (27R or 21R) of the polytype formed.

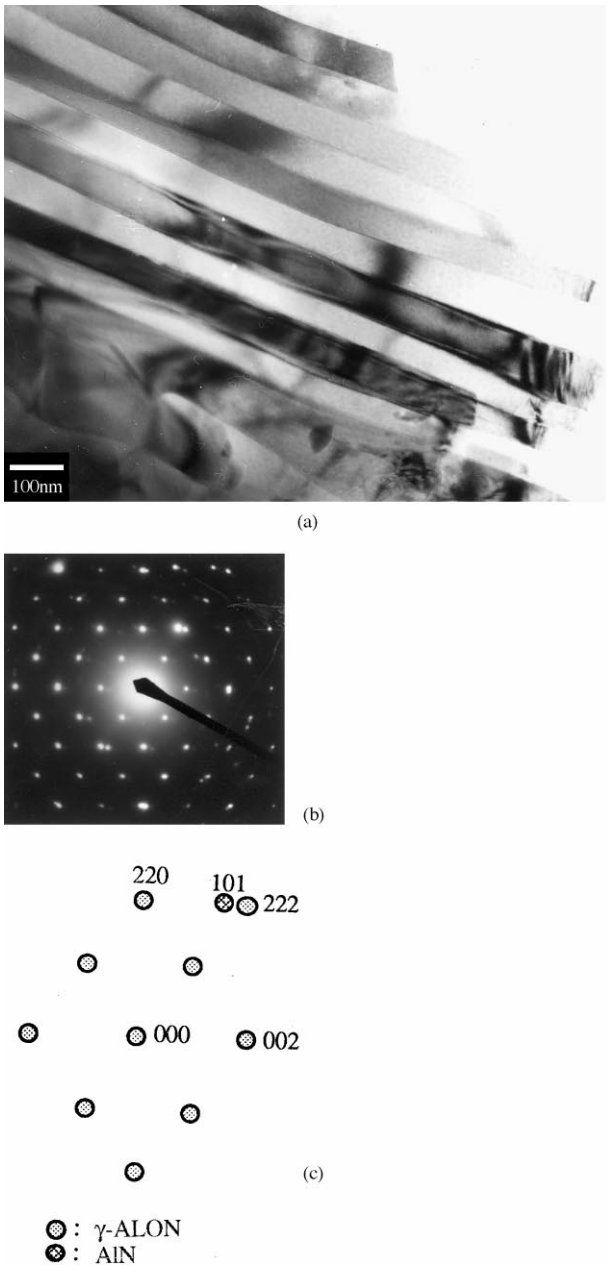

Fig. 7. Sample 1 slowly cooled ($R_c < 100$ K min^{-1}) (a) bright field electron micrograph showing the eutectoid B: AlN + γ-Alon; (b) electron diffraction pattern showing the orientation relationship between the 21R polytype, AlN and γ-Alon (one variant); (c) schematic representation of (b).

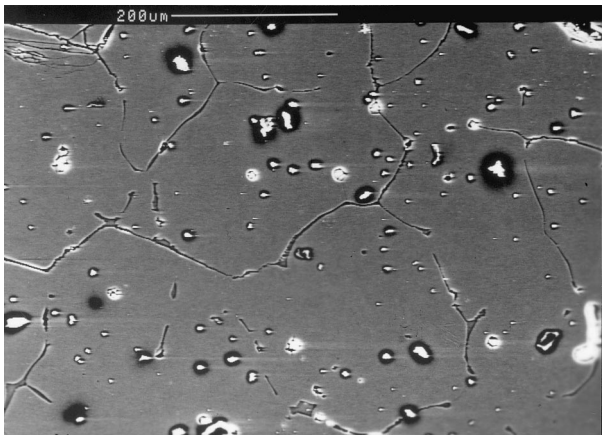

Fig. 8. Scanning back-scattered electron micrograph showing the equiaxed φ′ phase grains in sample 6 slowly cooled ($R_c < 100$°C min^{-1}).

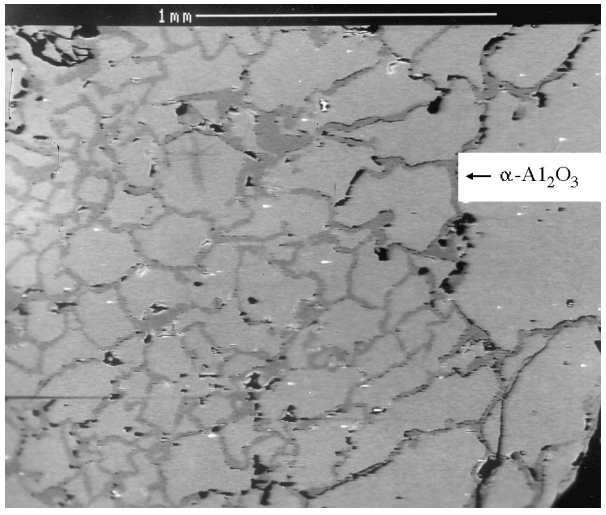

Fig. 9. Scanning back-scattered electron micrograph showing the microstructure of sample 7 water quenched composed of equiaxed δ grains with an intergranular precipitation of α-Al_2O_3.

The equilibrium temperature of the reactions (6) and (7) was estimated to be 2168 ± 15 K.

After a 2 h annealing at 2213 ± 10 K, the reaction (6) is entirely finished and the MSS material which underwent phase transformations during the heating becomes two phased 21R [resulting from reaction (6)] + γ-Alon. Above 2223 K, the 21R formation process is accelerated. During annealings at temperatures > 2323 K, the MSS material becomes two phased 12H [resulting from reaction (5)] + γ-Alon. During the heating preceding these annealings, a small quantity of 21R forms which transforms during the annealing by reaction (4) into 12H.

At 2173 ± 10 K, 21R is stable after 4 h 45 min, noted 21R S in Fig. 13. At 2313 K, 21R is stable after a shorter duration of 70 min, noted 21R S.

In a second step, the above formed phases were decomposed by using the thermal cycle (iii) as follows: On the MSS material of sample 1, during the heating followed by an annealing the phases 21R or 12H form, then during the temperature decrease followed by a new annealing those phases decompose. The decompositions occur in solid phase below 2173 K and their kinetics are maximum at 1973 K. Furthermore, we have noted that the kinetics of the eutectoid decomposition of the 21R

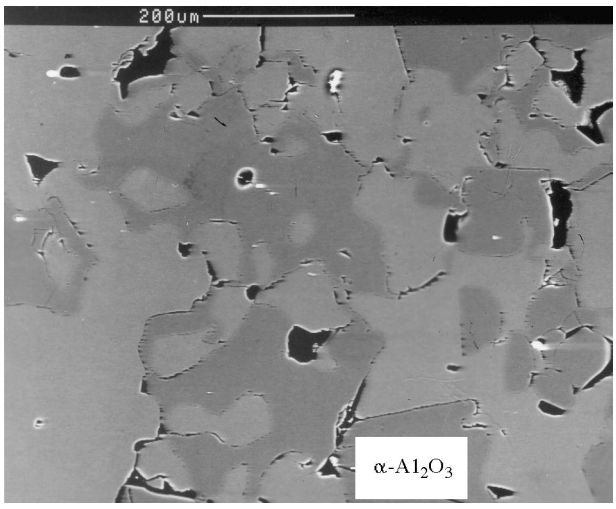

Fig. 10. Scanning back-scattered electron micrograph showing the microstructure of sample 7 water quenched composed of equiaxed δ and α-Al_2O_3 grains.

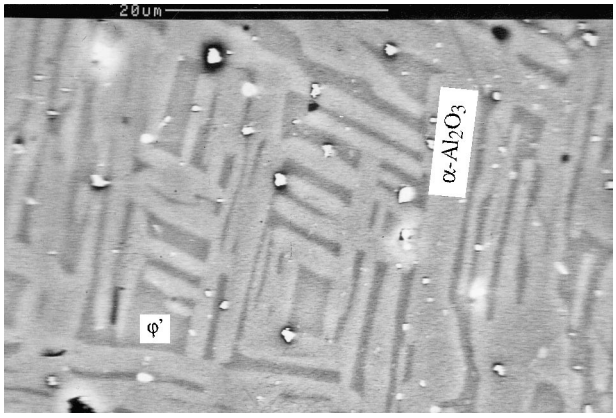

Fig. 11. Scanning back-scattered electron micrograph showing the microstructure of sample 7 annealed at 2223 K during 1 h. The δ phase is decomposed into φ′ + α-Al_2O_3.

and 12H phases depend on their previous formation mode, for example:

- A′ mode in solid phase: during the 1 h annealing at 2273 K, formation of 21R by reaction (6): AlN + γ-Alon→21R;
- B′ mode in liquid phase: during the 15 min annealing at 2403 K, formation of 21R by reaction (2):12H→21R + liquid;
- B′ mode in liquid phase: during the 15 min annealing at 2363 K, formation of 12H by reaction (2): 21R + liquid→12H.

The polytypes formed in the liquid phase (B′ mode) decompose more slowly than those formed in the solid phase (A′ mode).

3.2.1.2. Reaction (4). Reaction (4) was studied in the temperature stability range of 21R (between 2173 and 2318 K) then in that of 12 H (for temperatures between 2318 and 2358 K). The kinetics of reaction (4) is lower than the one of reaction (5). 12H remains metastable (noted 12H M in Fig. 13) after a 2 h annealing at 2273 K.

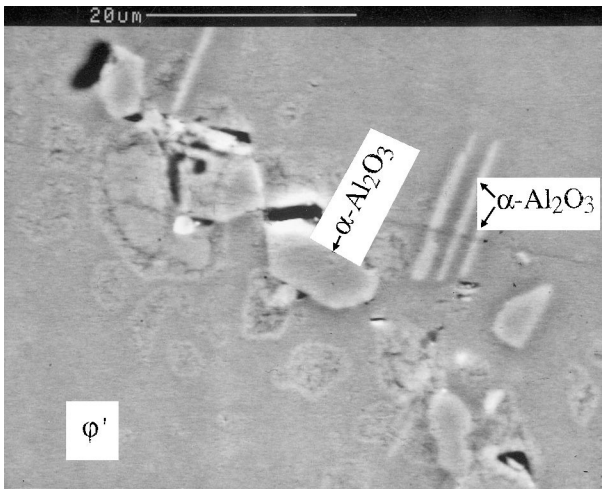

Fig. 12. Scanning back-scattered electron micrograph showing the microstructure of sample 6 annealed at 2123 K during 1 h. It will be noted the intergranular precipitation of α-Al_2O_3 either as hexagons or thin plates as a function of the section plane in the φ′ phase.

Table 6
Temperature of the peak onset of the different samples studied

Sample no.	$c_{average}$ (AlN mol%)	Peak onset ($T \pm 5$ K)
1	43.3	2358
2	36.3	2358
4	28.2	2315 (small peak)
5	21.3	2317
6	10.55	2316
7	3.5	2319

3.2.1.3. Reaction (3). The equilibrium temperature of the reaction (3) is estimated to be 2355 K but the 12H weight fraction which is involved in this equilibrium is so low that the reaction (3) is practically confused with the congruent melting (2358 K) of the γ-Alon spinel.

In Fig. 14(a) is shown the scanning back-scattered electron micrograph of sample 1 annealed at 2363 K for 15 min. During their dissolution in the liquid, the 12H polytype plates appear as fragments. In fact, during the heating, the eutectic melting occurs at 2358 K, and a small fraction of polytypes begin to dissolve, then when T increases from 2358 up to 2363 K, the liquid becomes enriched in nitrogen, and the weight fraction of 12H polytypes diminuishes compared to the one of the liquid.

3.2.1.4. Reaction (2). The equilibrium temperature of the reaction (2) is 2388 ± 10 K. At 2413 K, the formation

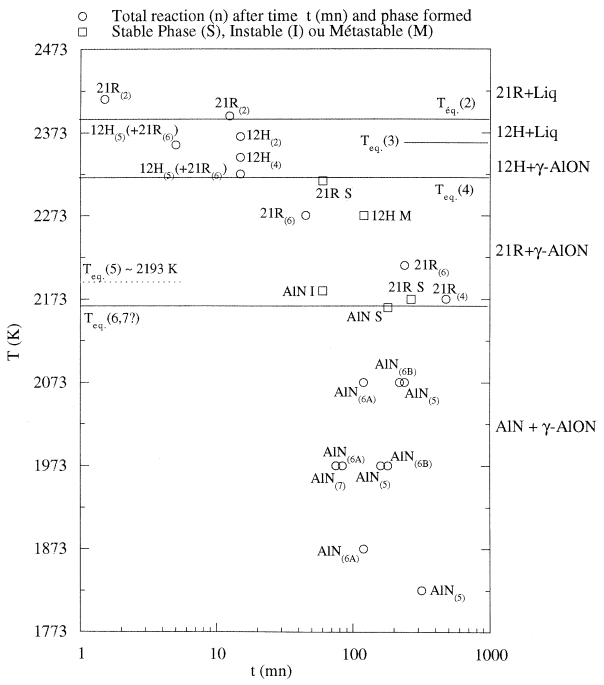

Fig. 13. Plot of the total duration of the reactions 2, 4, 5 and 6 versus temperature for AlN and the polytypes 27R, 21R and 12H.

of 21R is extremely fast and the time, after which the reaction is total plotted in Fig. 13, takes into account the one passed between 2388 and 2413 K during the heating. In Fig. 14(b) is shown the optical micrograph of sample 1 annealed at 2403 K for 10 min during which the 21R polytypes form.

3.2.1.5. Reaction (1). During the heating, the 21R polytype formed by reaction (2), melts instantaneously above 2573 K, then the 27R polytype precipitates up to 2673 K (temperature limit of our SETARAMTAG 24 device). During the ensuing cooling, the reaction 27R + liquid→21R occurs between 2573 and 2388 K in 2 min (R_c equal to 100 K min^{-1}). In order to keep 27R metastable, as shown in Fig. 1, it is necessary to use R_c higher than 700 K min^{-1} (i.e. about 15 s to go through the 185 K temperature range).

In Table 7 are listed the type and temperature of the reactions proposed involving the 27R, 21R and 12H polytypes.

The labels H and C refer to heating and cooling. The above reactions occur at temperature $T > T_{eq}$. during heating and at $T < T_{eq}$. during cooling. We have also indicated the reactions for which the equilibrium temperature is directly observed (noted: T_{eq} observed?: yes) and therefore is not situated in the stability range of another phase as it is the case when is mentioned: T_{eq} observed?, no.

The above equilibrium temperatures are now compared with the literature data.

- From Sakaï,[8] 27R is stable at 2173 K under N2 atmosphere. During annealings at low temperature (2183 K), we have not observed the decomposition of 21R in 27R + γ-Alon, but by taking into account the experimental temperature uncertainty (±30 K) on the decomposition of 12H, it is possible that 27R may form in the small temperature range between 2173 and 2193K, noted as T_{eq}(6,7?) in Fig. 13. As controversies exist in the literature, that hypothesis was used in the calculation of the AlN–Al_2O_3 pseudo-binary section.[4]
- Our experiments have shown that 21R is stable between 2181 to 2573 K. From Willems[11] 21R is stable from 2123 K. The data of MacCauley[12] (stability from 2163 K) seem underestimated when compared with ours, as it is the case for the equilibrium 21R + γ-Alon→12H[12] at 2263 K against

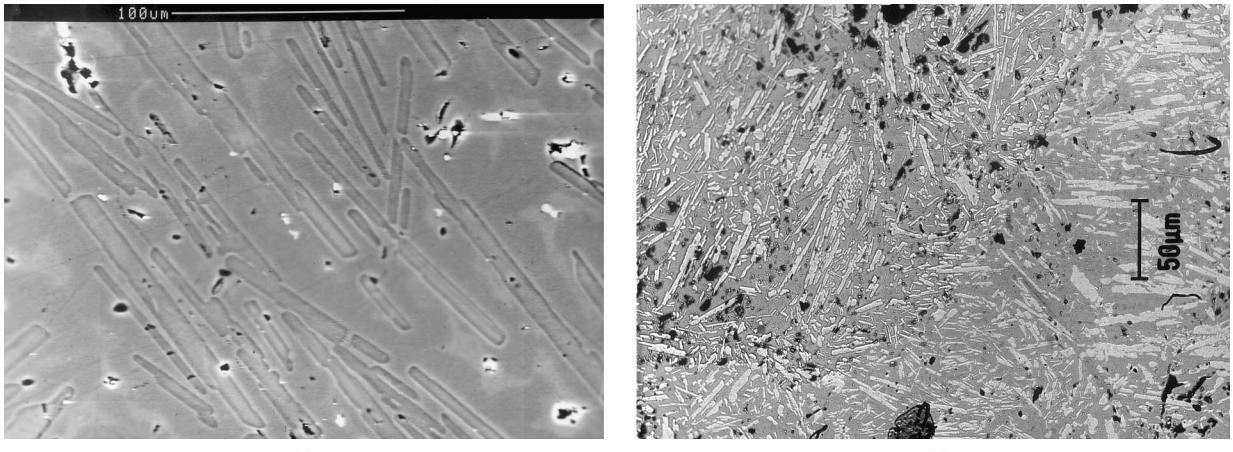

(a) (b)

Fig. 14. (a) Scanning back-scattered electron micrograph of sample 1, annealed at 2363 K during 15 min, showing the 12H polytypes; (b) optical micrograph of sample 1, annealed at 2403 K during 10 min, showing the 21R polytypes.

Table 7
Temperature and type of the reactions

Reaction no.	AlN	27R	21R	12H	Liquid	γ	T_{eq} (K)	Type	T_{eq} observed?
(1)		H	C		H		~2573	Peritectic	Yes
(2)			H	C	H		2388	Peritectic	Yes
(3)				C	H	C	2358	Eutectic	Yes
(4)			C	H		C	2318	Eutectoid	Yes
(5)	C			H		C	~2193	Eutectoid	No
(6)	C		H			C	2173/20	Eutectoid	No?
(7)	C	H				C	2173/20	Eutectoid	Yes?

2321 K (present work). In addition, Lejus[13] has mentioned the formation of a phase labelled X from 2123 K, which has been identified as 21R later on by Thompson.[14]

- We determined the temperature stability range of 12H between 2318 and 2388 K. This result is in agreement with Sakaï data[8] who determined that 21R is stable at 2273 K and 12H at 2323 K and with MacCauley data[15] who found that 21R is stable at 2308 K. However, for this latter, the temperature where 21R becomes stable again (2473 K) is higher than our result (2388 K).

By using the theoretical density of the phases and a γ-AlON spinel with 30 mol % AlN, we determined the mole (weight and volume) fractions of the products of the eutectoid reactions and the associated volume change (Table 8).

As for the 12H + liquid + γ-Alon equilibrium, MacCauley[15] proposed an eutectic reaction at 2358 K with a liquid having 53 mol% AlN and a congruent melting of γ-Alon spinel at 2438 K. Our experimental results are somewhat different. In fact, we have shown that the highest melting point of γ-Alon spinel is 2358 K. In addition, during the heating of a sample containing 44.5 mol AlN, after the melting point of γ-Alon spinel, the 12H polytypes remain solid and transform at 2388 K into 21R polytypes solid in the liquid. Furthermore, if the sample is then quenched, 12H, which could be produced during the eutectic solidification was not observed. Therefore, if the eutectic exists, it must involve a very small volume fraction of 12H. As we have seen that the greatest AlN content of γ-Alon is 35.5 mol%, the eutectic liquid composition must range between 39.5 and 35.5 mol% AlN.

3.2.2. γ-AlON

By electron microprobe analyses, we determined that the average maximum composition of γ-Alon spinel in sample 1 slowly cooled was equal to 35.5 ± 0.5 mol% AlN. By using the crystalline parameter found by X-ray diffraction and the composition/parameter dependence given by Willems[11] and Lejus,[13] a composition of 31.7 mol% AlN was determined. This composition discrepancy can be explained by the small composition variations resulting of the dendritic structure of solidification of sample 1. Our results are in satisfactory agreement with the data of Lejus[13] who found 32 mol% AlN at 2023 K and Willems[11] who claimed 34 mol% AlN at 2123 K with a continuous enlargement of the δ-Alon spinel range when the temperature is increasing.

The average minimum composition of γ-Alon spinel that we determined both by electron microprobe analyses and composition/parameter dependence in sample 5 slowly cooled was 23.5 ± 0.25 mol% AlN. The data of Willems[11] and Lejus[13] are lower: respectively, 19.5 at 2123 K and 16 mol% AlN at 2023 K.

The formation of the γ-Alon spinel at low temperature was observed at 1973 K by Sakaï[8] and MacCauley,[15] at 1923 K by Willems[11] and at 1873 K by Lejus.[13] This latter determined the decomposition of γ-Alon in AlN + α-Al_2O_3 at 1823 K. We did not succeed to observe such a decomposition between 1673 and 1873 K after a 100 min annealing.

The optimization of the thermodynamics parameters necessary to calculate the pseudo-binary AlN–Al_2O_3 section,[4] has used the data of Willems (1913 ± 10 K) as equilibrium temperature of the γ-Alon spinel decomposition.

Table 8
Mol weight and volume fractions of the components of the eutectoid reactions from 12H and 21R and volume change (calculated at room temperature)

Reaction no.	Start phase	Component 1				Component 2				ΔV/V (%)
			mol%	wt%	vol%		mol%	wt%	vol%	
(5)	12H	AlN	72.6	55.9	58.9	γ-Alon	27.4	44.1	41.1	−3.78
(6)	21R	AlN	75.7	60.4	63.3	γ-Alon	24.3	39.6	36.7	−2.68
(4)	12H	21R		92.6	93.3	γ-Alon		7.4	6.7	

3.2.3. φ′-Alon

In Fig. 10 is shown the microstructure of sample 6 annealed at 2123 K during 1 h. It will be noted the precipitation of α-Al_2O_3 either as hexagons or thin plates as a function of the section plane in the φ′ phase.

We determined:

- From sample 6, at 2313 K, a φ′-Alon composition ranges between 20 to 10.5 mol% AlN. MacCauley et al.[15] found an average composition equal to 16 mol AlN without formation of the δ phase and Michel[16] indicated 16.7 mol% AlN.
- At low temperature, in sample 7 that δ decomposes into φ′ + α-Al_2O_3 at 2203 ± 15 K while Lejus[13] claimed that δ decomposes into γ + α-Al_2O_3 at 2173 K. In fact, she reported the observation of undisturbed X-ray diffraction peaks of γ-Alon spinel up to 2173 K. For higher temperatures, she observed a splitting in two of some peaks that she attributed to a continuous deformation of the γ-Alon spinel crystalline lattice. This phenomenon could be explained by the progressive formation of the φ′ peaks slightly shifted from the γ-Alon spinel ones. In addition, 2173 K may be underestimated of about 50 K as she reported 2123 K as temperature of formation of the polytypes against about 2173 K.

Goeuriot[17] observed non-identified X-ray diffraction peaks attributed to a δ + θ mixture from 2053 K. A further examination of the spectrum reveals the presence of the φ′ phase. In another paper, Goeuriot[18] reported the melting of these samples at 2173 K (against about 2323 K in the present work) and the formation of γ at 1823 K. A shift in temperature for those results seems possible.

Bassoul et al.[19] have reported that, in the systems Ga_2O_3–MgO, Al_2O_3–NiO, Al_2O_3–AlN and Al_2O_3–Li_2O, γ-Alon spinel non-stochiometric can be obtained by water quench and by slower cooling, the ε phase (in fact φ′) forms rapidly, just below the limit of the composition stability range of the γ-Alon spinel. The samples, having a composition range between 80 and 85 mol% Al_2O_3, are then two-phased: φ′ + γ-Alon spinel non-stochiometric. On the contrary, during annealings at lower temperature, φ′ does not form and the two phase equilibrium Al_2O_3–AlN is reached.

It seems that Sakaï[8] did not know of the existence of the φ′ phase, but he observed the presence of a phase (noted Y) different of δ from 2198 K for average compositions of 15 to 20 mol% AlN. It seems probable that this Y phase is φ′ by taking into account the shift (estimated between 0 and 30 K) in Sakaï's temperatures: in fact he reported the γ-Alon spinel melting point at 2353 K (against 2358 K in the present work) and that of Al_2O_3 at 2298 K (against 2327 K). So the more probable temperature of formation of φ′ seems to be between 2198 and 2228 K.

In our experiments, we have shown that γ-Alon spinel never has a composition lower than 23.5 mol.% AlN even when obtained by quench at 700 K min^{-1}, so φ′ must be stable until melting.

3.2.4. φ′ Decomposition into γ-Alon and α-Al_2O_3

We did not succeed in obtaining such a decomposition from sample 6 either slowly cooled (R_c = 2 K min^{-1}) or annealed between 2123 and 1673 K for 1 to 18 h. φ′ seems metastable whatever the temperature.

3.2.5. δ Phase

We determined:

- by electron microprobe analyses, in sample 7 slowly cooled, the AlN lower content of δ equal to 5.5 mol% AlN. The AlN higher content was situated at about 9.5 mol% because the AlN lower content of φ′ was measured equal to 10.5%. These results are in agreement with the one of Michel[16] who indicated 10 mol% AlN. From 2 mol% AlN, Lejus[13] observed the formation of α-Al_2O_3.
- at low temperature that δ decomposes into φ′ + α-Al_2O_3 between 2253 and 2203 K. One hour is necessary to obtain this decomposition, see (Fig. 11). Previously, Lejus[13] observed its decomposition into γ + α-Al_2O_3 at 2173 K as mentioned above.

4. Conclusion

The samples enriched in nitrogen contain polytypes the type of which (27R, 21R and 12H) is a function of the cooling rate used from the melting. These polytypes can decompose eutectoidally into AlN and γ-Alon spinel. Two types of eutectoid have been observed.

The nitrogen less rich samples are composed of γ-Alon spinel, φ′, δ and/or corundum.

The composition and temperature ranges of the different phases have been determined by performing different annealings. The main differences with data of literature are the following:

- existence of a less marked eutectic between the 21R polytype, the liquid and γ-Alon spinel. The eutectic temperature and composition are very near those of the congruent melting of γ-Alon spinel.
- A stability range of the 27R polytype with the liquid was determined for temperatures about 2573 K.
- The formation temperature of the φ′ and δ phases was measured respectively equal to 2198 and 2253 K.

Acknowledgements

The authors are indebted to Dr. G. André of the Laboratoire Léon Brillouin du Centre d'Etudes de Saclay for neutron experiments.

References

1. Tabary, P. and Servant, C., Crystalline and microstructure study of the $AlN–Al_2O_3$ section in the Al–N–O system, I. Polytypes and γ-Alon spinel phase. *J. Appl. Cryst*., 1999, **32**, 241–252.
2. Tabary, P. and Servant, C., Crystalline and microstructure study of the $AlN–Al_2O_3$ section in the Al–N–O system, II. φ′ and δ-Alon spinel phase. *J. Appl. Cryst*., 1999, **32**, 253–272.
3. Tabary, P., Servant, C. and Guymont, M., High resolution transmission electron microscopy study of the φ′ and δ-Alon spinel phases of the pseudo-binary section $AlN–Al_2O_3$. *J. Appl. Cryst*., 1999, **32**.
4. Tabary, P. and Servant, C., Thermodynamic assessment of the pseudo-binary section $AlN–Al_2O_3$. *Calphad*, 1998, **22**(2), 179–201.
5. Jack, K. H., Review: sialons and related nitrogen ceramics. *J. Mater. Sci*., 1976, **11**, 1135–1158.
6. Rietveld, H. M., A profile refinement method for nuclear and magnetic structures. *J. Appl. Cryst*., 1969, **2**, 65–71.
7. Rodriguez, J., *Manual of the Computer Program*, 1994.
8. Sakai, T., Hot pressing of the $AlN–Al_2O_3$ system. *J. Ceram. Assoc. Japan (Yogyo Kyokai Shi)*, 1978, **86**, 125–130.
9. Porter, D. A. and Easterling, K. E., Solidification. In *Phase Transformation in Metals and Alloys* 2nd edn, Chapman and Hall, 1993.
10. Bassoul, P., Lefebvre, A. and Gilles, J. C., Structures á antiphases périodiques des phases intermédiaires apparaissant lors de la décomposition du spinelle non-stoechiométrique dans les systémes $Ga_2O_3–MgO$, Al_2O_3-NiO. *J. Sol. Stat. Chem*., 1974, **10**, 56–65.
11. Willems, H. X., Hendrix, M. M. R. M., de With, G. and Metselaar, R., Thermodynamics of Alon II: Phase relations. *J. Eur. Ceram. Soc*., 1992, **10**, 339–346.
12. MacCauley, J. W. and Corbin, N. D., Phase relations and reaction sintering of transparent cubic aluminium oxynitride spinel (Alon). *J. Am. Ceram. Soc*., 1979, **62**(9–10), 476–479.
13. Lejus, A., Sur la formation á haute température de spinelles non stoechiométriques et de phases dérivées dans plusieurs systèmes d'oxydes à base d'alumine et dans le système alumine-nitrure d'aluminium. *Rev. Int. Hautes Tempér. et Réfract*., 1964, **1**, 53–95.
14. Thompson, D. P., Roebuck, P., Rae, A. W. J. M. and Jack, K. H., Unpublished work presented to Journées d'Etude sur les Nitrures II, U.E.R des Sciences, Limoges, 1975.
15. MacCauley, J. W. and Corbin, N. D., High temperature reactions and microstructures in the $Al_2O_3–AlN$ system. In *Progress in Nitrogen Ceramics*. Martinus Nijhoff Publishers, 1983, pp. 111–118
16. Michel, D., *Rev. Int. Hautes Tempér. et Réfract*., 1972, **9**(2), 225–242.
17. Goeuriot-Launay, D., Goeuriot, P., Thévenot, F. and Carry, C., Structural evolution of alumina-γ-aluminium oxynitride composites during high-temperature compression creep. *J. Mat. Sci*., 1992, **27**, 358–364.
18. Goeuriot-Launay, D., Goeuriot, P., Thévenot, F., Orange, G., Fantozzi, G., Trabelsi, R. and Treheux, D., Effect of γ-aluminum oxynitride dispersion on some alumina properties. *Ceram. Int*., 1989, **15**, 207–212.
19. Bassoul, P., Lefebvre, A. and Gilles, J. C., Phases ε obtenues par decomposition des spinelles non-stoechiométriques dans les systĕmes $Ga_2O_3–MgO$, $Al_2O_3–NiO$, $Al_2O_3–AlN$ et $Al_2O_3–Li_2O$. *Mat. Res. Bull*., 1976, **11**, 11–14.